^{1}H, ^{13}C, and ^{15}N NMR Resonance Assignments, Secondary Structure, and Backbone Topology of a Variant of Human Interleukin-3

Yiqing Feng,* Barbara K. Klein, Linh Vu, Serdar Aykent, and Charles A. McWherter*

G. D. Searle and Company, 700 Chesterfield Parkway North, St. Louis, Missouri 63198

Received December 8, 1994; Revised Manuscript Received February 1, 1995[⊗]

ABSTRACT: Interleukin-3 (IL-3) is a cytokine which stimulates the proliferation and differentiation of hematopoietic progenitors into multiple cell lineages. The ^{1}H, ^{15}N, and ^{13}C NMR resonances of a recombinant human IL-3 variant (SC-65369) have been assigned using two- and three-dimensional NMR techniques on uniformly $^{13}C/^{15}N$-enriched protein. Five helical segments (residues 16−26, 42−50, 55−65, 73−82, and 104−120) and three reverse turns (residues 51−54, 68−71, and 87−90) were identified from the pattern of sequential NOE connectivities, NH(i)−C$^{\alpha}$H(i) scalar coupling constants ($^{3}J_{NH\alpha}$), amide hydrogen exchange data, and the deviation of $^{13}C^{\alpha}$, $^{13}C^{\beta}$, ^{13}CO, and C$^{\alpha}$H chemical shifts from random-coil values. Long-range NOEs indicate that the global folding pattern of human IL-3 is a four-helical bundle with an up-up-down-down arrangement of helices that is similar to that of other members of the cytokine family, such as granulocyte-macrophage colony stimulating factor (GM-CSF). A fifth short helix (helix A′, residues 42−50) is located in the loop connecting the first and second helices. The absence of helix A′ in the corresponding structures of GM-CSF and interleukin-5 suggests that it may be important for recognition of IL-3 by its receptor. The existence of at least two forms of the protein that differ in local conformation was implied from the observation of a limited set of doubled resonances in which each doublet partner had a similar pattern of short-, medium-, and long-range NOEs. The majority of the doubled resonances were close in sequence or space to a proline-rich sequence, which suggested that the different conformational forms of SC-65369 may be caused by slow *cis*−*trans* isomerization of proline peptide bonds.

Interleukin-3 (IL-3)[1] is a protein that belongs to a subfamily of cytokines which regulate proliferation, differentiation, and activation of hematopoietic cells [for reviews, see Schrader (1986), Yang and Clark (1990), and Metcalf (1991)] through signal-transducing cell surface receptors. Stimulation of IL-3 receptors on multipotent hematopoietic progenitors, and certain lineage restricted progenitors, results in the expansion and differentiation of hematopoietic cell lineages, leading to the proliferation of essential, terminally differentiated blood cells including platelets, basophils, eosinophils, and neutrophils. In addition, recombinant human IL-3 (hIL-3) stimulates histamine release by basophils (Haak-Frendscho et al., 1988), degranulation of eosinophils (Lopez et al., 1989), and primes peripheral blood leukocytes for the production and release of sulfidoleukotrienes. Although hIL-3 has shown some promising results in the treatment of chemotherapy-induced neutropenia and thrombocytopenia (Ganzer et al., 1990; Herrmann et al., 1992; Ganzer, 1993), the intrinsic proinflammatory effect of hIL-3 on end-stage leukocytes may result in a narrow therapeutic index (Biesma et al., 1992; Denzlinger et al., 1993). Extensive mutagenesis of truncated hIL-3 has led to molecules with 10−20-fold greater proliferative and colony forming activity relative to hIL-3, but with only a 2-fold increase in potentiation of histamine and sulfidoleukotriene release (Olins et al., 1995; Thomas et al., 1995).

Among the hematopoietic growth factors, IL-3 is most closely related to the short-chain cytokines GM-CSF and IL-5 [reviewed by Goodall et al. (1993) and Miyajima et al. (1993)] whose receptors share a common β-subunit with the IL-3 receptor (Kitamura et al., 1991; Tavernier et al., 1991). The three-dimensional structures of both GM-CSF and IL-5 were published recently (Diederichs et al., 1991; Walter et al., 1992; Milburn et al., 1993). GM-CSF is folded into a four-helical bundle in which the first two helices are roughly parallel to one another with a long loop connecting them, and the last two helices form a second parallel pair that is also connected by a long loop, and these two sets of parallel helices are arranged approximately antiparallel to one another. IL-5 exists as a dimer with an interesting variation of the four-helical bundle structure (Milburn et al., 1993): Each of the two four-helical bundles in the structural dimer is composed of a single C-terminal helix from one chain and three N-terminal helices from the other chain. The four-helix bundle motif is common among many other growth factors such as IL-2 (Bazan, 1992; McKay, 1992; Mott et al., 1992), IL-4 (Smith et al., 1992; Powers et al., 1992a; Wlodawer et al., 1992), M-CSF (Pandit et al., 1992), G-CSF

* Address correspondence to either author at Searle Discovery Research, c/o Monsanto Co., Mail Zone BB3G, 700 Chesterfield Parkway North, St. Louis, MO 63198.

[⊗] Abstract published in *Advance ACS Abstracts,* May 1, 1995.

[1] Abbreviations: IL-3, interleukin-3; hIL-3, human IL-3; SC-65369, a truncated variant of hIL-3 mutated in 14 of 112 positions; GM-CSF, granulocyte-macrophage colony stimulating factor; IL-5, interleukin-5; IL-2, interleukin-2; IL-4, interleukin-4; G-CSF, granulocyte colony stimulating factor; M-CSF, macrophage colony stimulating factor; LIF, leukemia inhibitory factor; NOE, nuclear Overhauser effect; $^{3}J_{NH\alpha}$, intraresidue three-bond scalar coupling constant between NH and C$^{\alpha}$H; CHES, 2-(*N*-cyclohexylamino)ethane; DTT, DL-dithiothreitol; SDS−PAGE, sodium dodecyl sulfate−polyacrylamide gel electrophoresis; HOAc-d_4, acetic acid-d_4; Xaa, any of the 20 amino acids commonly found in proteins.

0006-2960/95/0434-6540$09.00/0

(Hill et al., 1993; Lovejoy et al., 1993; Zink et al., 1992, 1994; Werner et al., 1994), somatotropin (Abdel-Meguid et al., 1987; de Vos et al., 1992), and LIF (Robinson et al., 1994). hIL-3 purified from *Escherichia coli* (Freeman et al., 1991) as a 133 amino acid residue, single disulfide cross-linked polypeptide was found to be insoluble in the concentration and pH range required for NMR studies (J. Likos and C. McWherter, unpublished experiments). Despite a considerable effort, neither an X-ray nor an NMR structure of hIL-3 has yet been reported.

In order to understand the structure−function relationships of hIL-3, we initiated a project to determine the three-dimensional structure of a soluble variant of hIL-3 using multidimensional heteronuclear NMR techniques. In an effort to discover a molecule with increased separation between proliferative and proinflammatory activities, hundreds of hIL-3 variants were generated by saturation mutagenesis at multiple sites distributed throughout the sequence (Olins et al., 1995). A number of active variants recovered with high yield provided a pool for solubility screening, and several among these were found to have a solubility significantly greater than that of hIL-3. The present study focused on a 112-residue truncated variant of recombinant hIL-3, SC-65369, which lacks the N-terminal 13 residues and C-terminal 8 residues, and which has 14 amino acid substitutions relative to the wild-type protein. The characterization of SC-65369, which will be described in detail elsewhere (P. Olins, C. Bauer, and J. Thomas, unpublished results), revealed that it has slightly higher activity than native IL-3 in cell proliferation assays and comparable affinity for the low-affinity (α-subunit) receptor. In this paper, we report the ^{1}H, ^{15}N, and ^{13}C NMR resonance assignments, the secondary structure, and the chain-folding topology of SC-65369.

EXPERIMENTAL PROCEDURES

Sample Preparation. SC-65369 (P. Olins and C. Bauer, unpublished results) is a variant of hIL-3 which consists of residues 14−125 of the wild-type sequence (Yang et al., 1986) with the following substitutions: V14A, N18I, T25H, Q29R, L32N, F37P, G42S, Q45M, N51R, R55T, E59L, N62V, S67H, and Q69E. This protein was produced in refractile bodies by expression of the plasmid pMON 13302 in *E. coli* strain JM101. For each of the samples prepared in this study, small amounts of cells were grown overnight, and these were used to inoculate 300 mL of media in flasks at a 1:40 ratio. The inoculated cultures were grown at 37 °C for about 3 h before induction with nalidixic acid (50 μg/mL), and cells were harvested 4 h after induction. The ^{15}N-labeled protein was produced by growing the cells on minimal medium M9 (Maniatis et al., 1982) containing 1 g/L of U-^{15}N (99 atom %) ammonium chloride (Cambridge Isotope Laboratory, Woburn, MA) as the sole nitrogen source and supplemented with glucose at 5 g/L as the carbon source. In a similar way, the $^{13}C,^{15}N$-labeled protein was prepared using M9 supplemented by U-^{15}N (99 atom %) ammonium chloride as the sole nitrogen source (1 g/L) and U-$^{13}C_6$ (99 atom %) glucose (5 g/L, fermentation grade, Martek Biosciences Corporation, Columbia, MD) as the sole carbon source. Harvested cells were washed and stored at −70 °C.

Thawed cells were sonicated, and refractile bodies were isolated by centrifugation. Refractile bodies containing SC-65369 were extracted using a 50 mM CHES buffer, pH 9.5, containing 6 M guanidine-HCl, and 0−30 mM DTT, and the extracted protein was folded by sequential dialysis against 50 mM CHES buffers containing 4 M and 2 M guanidine-HCl at pH 8.0. The folded protein was purified using a Vydac 1- × 25-cm C_{18} reverse-phase column (218TP510; Separations Group, Hesperia, CA) and a mobile phase consisting of solvents A (0.1% TFA/H_2O) and B (0.1% TFA/CH_3CN). The folding reaction products were applied to the column in 20% solvent B at a flow rate of 3 mL/min for 10 min, followed sequentially by linear gradients in solvent B from 20 to 40% in 10 min and 40 to 50% in 50 min. The column effluent was monitored at 280 nm, and pure product fractions were identified by analytical-scale HPLC. Pure fractions from several runs were pooled, frozen, and lyophilized. In some cases, an S-Sepharose (Pharmacia, Piscataway, NJ) column was used as a final step to remove a small amount of high molecular weight material that had been observed by SDS−PAGE. When necessary, the HPLC-purified fractions were applied to the S-Sepharose column equilibrated with 20 mM sodium acetate, pH 5.5, containing 50 mM NaCl. After washing extensively with the same buffer, pure SC-65369 was eluted with the sodium acetate buffer containing 100 mM NaCl.

The purified SC-65369 was greater than 95% homogeneous as determined by analytical HPLC. The samples were also characterized by reducing SDS−PAGE, electrospray mass spectrometry, and tryptic peptide mapping. The isotopic substitution was determined to be greater than 99% for both ^{15}N- and $^{13}C,^{15}N$-labeled samples by mass spectrometry. Samples for NMR spectroscopy were about 0.8−1.0 mM SC-65369 in a buffer consisting of 5 mM HOAc-d_4 in either 95% H_2O/5% D_2O or 99.9% D_2O at a pH* (uncorrected) of 4.6.

NMR Spectroscopy. All NMR spectra were recorded at 30 °C on a triple-resonance Varian UNITY-500 spectrometer operating at a nominal proton frequency of 500 MHz and equipped with three waveform generators, a pulsed-field gradient unit, and a 5 mm triple-tuned probe. Typical spectral widths were 6400, 1265, 2500, 1420, and 7500 Hz in ^{1}H, ^{15}N, $^{13}C^{\alpha}$, ^{13}CO, and aliphatic ^{13}C dimensions, respectively. The resolution in HCCH-COSY, HCCH-TOCSY, ^{13}C-edited NOESY, and simultaneous $^{13}C,^{15}N$-edited NOESY experiments was increased by setting the spectral width for aliphatic ^{13}C to 2600 Hz and folding in resonances which fall outside of the spectral window. Carrier frequencies for heteronuclei were set to 121 ppm for ^{15}N, 59 ppm for $^{13}C^{\alpha}$, 44 ppm for $^{13}C^{\alpha}/^{13}C^{\beta}$, 176 ppm for ^{13}CO, and 41.5 ppm for aliphatic ^{13}C.

Three-dimensional ^{15}N-edited TOCSY-HMQC (Marion et al., 1989a), ^{15}N-edited NOESY-HMQC (Marion et al., 1989b; Zuiderweg & Fesik, 1989), 3D ^{15}N-edited HMQC-NOESY-HMQC (Ikura et al., 1990), and 2D $^{15}N-^{1}H$ HMQC-J experiments (Kay & Bax, 1990) were acquired on an ^{15}N-labeled sample dissolved in 95% H_2O/5% D_2O buffer. Solvent suppression was achieved by low-power preirradiation with the carrier frequency placed on the water peak. Three-dimensional HNCO (Kay et al., 1990), HNCA (Kay et al., 1990), HN(CO)CA (Bax & Ikura, 1991), CBCA(CO)NH (Grzesiek & Bax, 1992a), CBCANH (Grzesiek & Bax, 1992b), HBHA(CBCACO)NH (Grzesiek & Bax, 1993a), C(CO)NH (Grzesiek & Bax, 1993b), H(CCO)NH (Grzesiek & Bax, 1993b), (HB)CBCA(COCA)HA (Kay, 1993; modi-

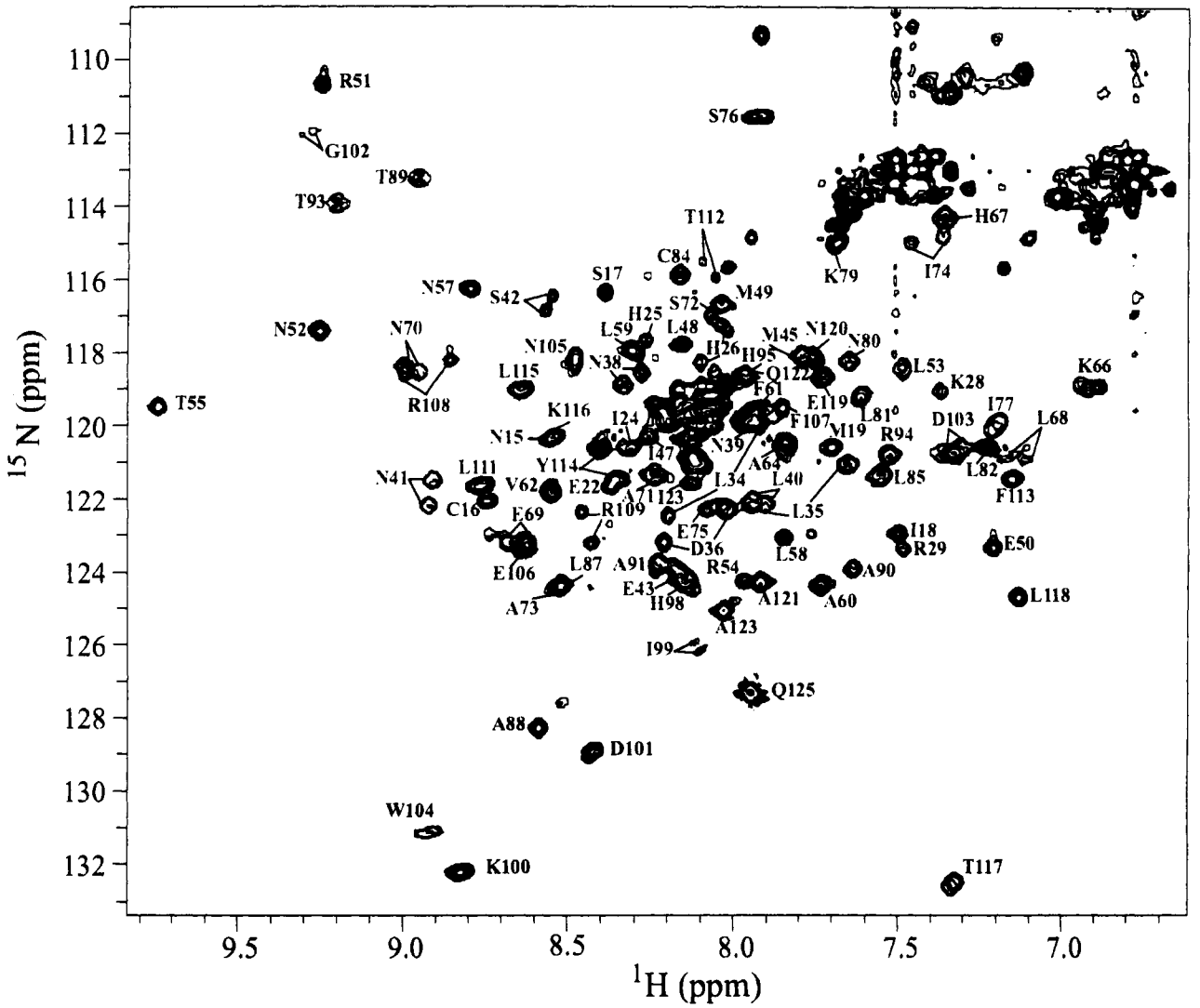

FIGURE 1: 2D ^{15}N−^{1}H HMQC spectrum of uniformly ^{15}N-labeled SC-65369 with the residue assignments indicated next to the cross-peaks. Some cross-peaks that occur in severely crowded regions are not labeled for the sake of clarity. The spectral heterogeneity is evident for a number of residues which are assigned to two cross-peaks. The cross-peaks for R51 and T117 are folded in from outside the ^{15}N spectral window.

fied for use without gradients), HCA(CO)N (Kay et al., 1990; Powers et al., 1991), HCCH-COSY (Bax et al., 1990), HCCH-TOCSY (Bax et al., 1990), ^{13}C-edited NOESY-HMQC (Ikura et al., 1990), simultaneous ^{13}C,^{15}N-edited NOESY-HSQC (Pascal et al., 1994), and two-dimensional carbonyl-edited ^{13}C-^{1}H HSQC (Grzesiek & Bax, 1993a) experiments were recorded on a uniformly ^{13}C,^{15}N-labeled sample in 95% H_2O/5% D_2O or D_2O buffer. Solvent suppression was achieved by low-power preirradiation at the solvent frequency, by spin-lock pulses (Messerle et al., 1989), or by a combination of the two. In the simultaneous ^{13}C,^{15}N-edited NOESY-HSQC experiment (Pascal et al., 1994), the H_2O signal was suppressed by the gradient pulses. Relaxation delays in all experiments were 0.8−1.0 s. Quadrature detection in all indirectly detected dimensions was achieved using the States−TPPI method (Marion et al., 1989c). Due to limited solubility of SC-65369, extensive signal-averaging was necessary and each experiment took 5−7 days to complete. Acquisition and processing details for each experiment are listed in Table 1 in the Supplementary Material. Gaussian multiplication of data was used in the acquisition dimensions. In some data sets, the indirectly acquired dimensions were extended by the linear prediction method as implemented in NMRz or Triad (Tripos Associates, St. Louis, MO). The data in the indirectly detected dimensions were apodized with a shifted (60−80°) squared-sine bell prior to zero-filling and Fourier transformation.

Hydrogen exchange data were collected on a U-^{15}N-labeled sample at 15 °C in order to slow the exchange rate and thereby detect somewhat faster exchanging amide protons. Prior to the exchange experiments, ^{15}N−^{1}H HSQC spectra (Bodenhausen & Ruben, 1980) of an ^{15}N-labeled sample in 95% H_2O/5% D_2O were collected at 30, 22, and 15 °C in order to map the assignments at 30 °C to the spectrum recorded at 15 °C. The exchange was initiated by dissolving an unexchanged, lyophilized sample in D_2O buffer and the first in a series of ^{15}N−^{1}H HSQC spectra (ca. 9 min/each) was recorded within 10 min of the initial dissolution. Additional spectra were collected at various intervals over the next 29 h.

Two-dimensional NMR spectra were processed and analyzed using the VNMR software package (Varian Instruments, Palo Alto, CA). $^{3}J_{NH\alpha}$ coupling constants were extracted from ^{15}N−^{1}H HMQC-J data (Kay & Bax, 1990;

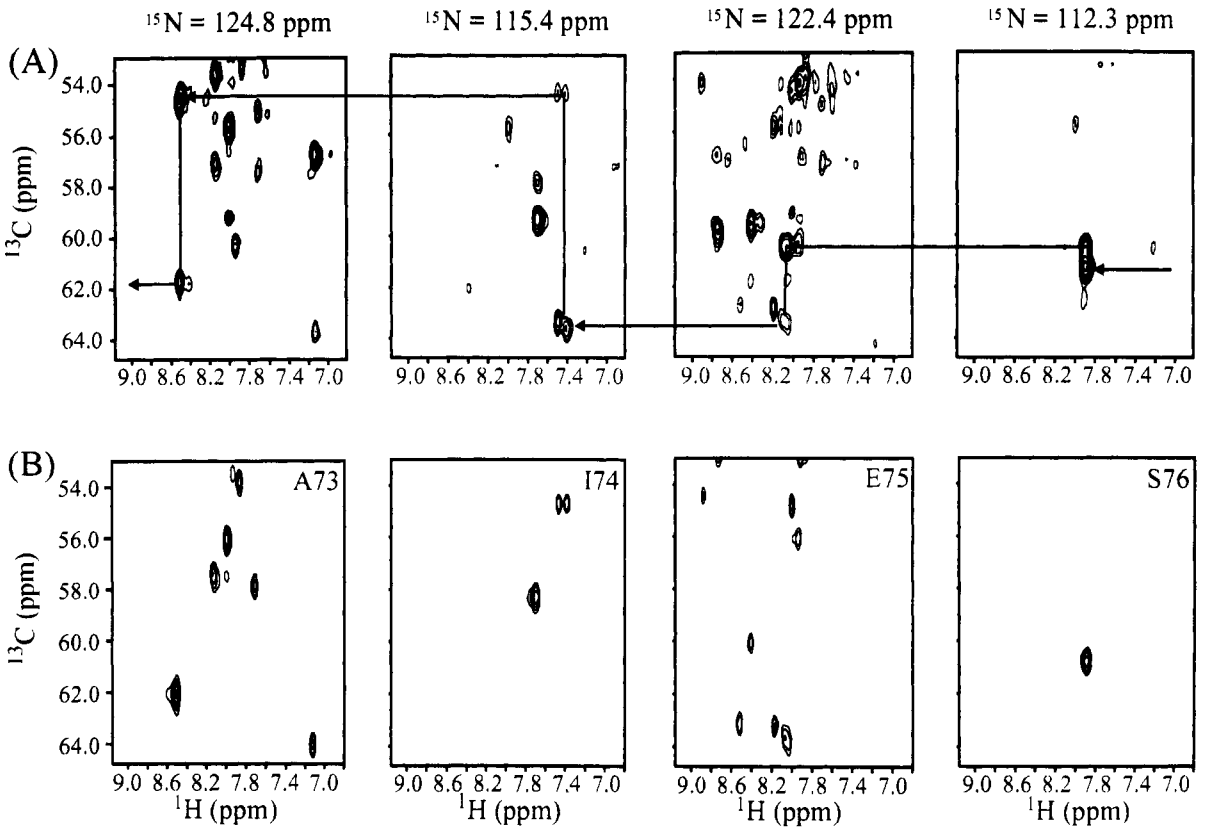

FIGURE 2: 2D planes of 3D HNCA (A) and HN(CO)CA (B) illustrating the connectivities of residues 73−76 in SC-65369. An example of the heterogeneity is apparent in the doublet for the NH and, to a lesser extent, the C^{α} resonances of I74.

Forman-Kay et al., 1990) for those cross-peaks that had observable splittings following Gaussian t_1 apodization for at least three of the seven tested parameter sets. Three-dimensional NMR spectra were processed and analyzed using NMRz or Triad (Tripos Associates) on a Sun workstation. The consensus secondary chemical shift index was calculated using the program CSI (Wishart & Sykes, 1994).

RESULTS AND DISCUSSION

2D ^{15}N−^{1}H Chemical Shift Correlation Maps and Chemical Shift Heterogeneity. The 2D ^{15}N−^{1}H HMQC spectrum of uniformly ^{15}N-labeled SC-65369 and the residue cross-peak assignments are shown in Figure 1. Narrower than average line widths for five signals in this spectrum were found to belong to the C-terminal residues 121−125. Despite a considerable range in ^{15}N chemical shifts, and the relatively small size of SC-65369, there is nonetheless inadequate resolution of many cross-peaks. Particularly troublesome were many apparently isolated cross-peaks that on closer inspection turned out to be two closely overlapping cross-peaks with comparable intensities (e.g., D101 and W104 in Figure 1), suggesting either chemical or conformational heterogeneity. The extent of heterogeneity became obvious upon comparison of either the HN(CO)CA and HNCA or the CBCA(CO)NH and CBCANH spectra. Similar heterogeneity was subsequently observed in the ^{1}H spectra of three other hIL-3 variants (data not shown). Electrospray mass spectrometry of natural-abundance, ^{15}N-, and ^{13}C,^{15}N-enriched samples of SC-65369 determined that each sample contained a single predominant mass species that was close to that calculated from the expected isotopic substitution (data not shown). In addition, mass spectral analysis of HPLC-resolved tryptic fragments at a resolution (1 amu) sufficient to detect subtle chemical differences, such as deamidation of Asn and Gln side chains, was able to account for the entire sequence. Furthermore, similar mass spectral results have been obtained on other hIL-3 variants which show spectral heterogeneity. Taken together, these results indicate that the protein is a single chemical species and that it is therefore reasonable to attribute the heterogeneity to two or more conformational forms of the protein. The available NMR data (see below) suggest that isomerization of one or more of the nine prolines is a possible explanation for the origin of the heterogeneity. Several additional explanations that are considered less likely, but are not yet excluded, include a monomer−dimer equilibrium, the binding of metal ions, and rotational isomerism of the disulfide bond.

Main-Chain Sequential Assignments. Site-specific sequential assignment of SC-65369 was carried out using a combination of double- and triple-resonance 3D NMR experiments. The assignment strategy was similar to that described by Powers et al. (1992b). However, a number of more recently developed experiments that provide multiple correlations to main-chain resonances [e.g., CBCA(CO)NH and C(CO)NH] were found to be useful in overcoming the spectral degeneracy and heterogeneity observed with SC-65369. The main-chain assignment procedure began with experiments that correlated amide nitrogen and amide proton resonances with those of backbone and side-chain nuclei which are in the same and nearest-neighbor residues [^{15}N-edited TOCSY-HMQC, HN(CO)CA, HNCA, CBCA(CO)-NH, CBCANH, HBHA(CBCACO)NH]. Carbonyl carbons were assigned by matching the HNCO cross-peak frequencies to amide proton and nitrogen frequencies from the first set

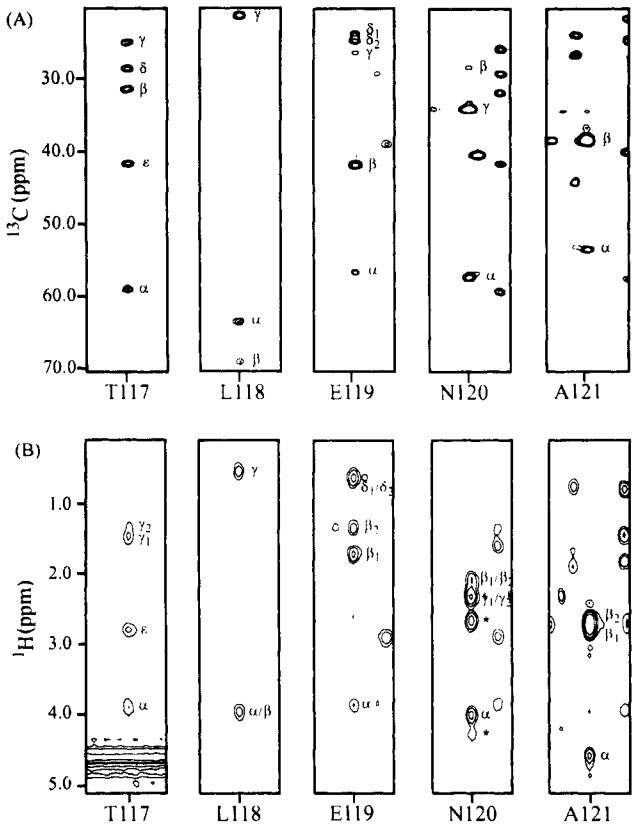

FIGURE 3: Portions of the 3D C(CO)NH (A) and 3D H(CCO)NH (B) spectra illustrating the correlations observed between the amide and the aliphatic side-chain carbon or proton resonances of the preceding residues for residues 117−121. The cross-peaks marked with an asterisk are from adjacent planes.

of experiments. After most of the main-chain resonances were assigned, the (HB)CBCA(COCA)HA and HCA(CO)N spectra, in combination with that of the HNCO experiment, were used to confirm the assignments as well as to resolve ambiguities and locate any missing N(i)−NH(i) correlations. Finally, the assignments were further verified using data from 2D carbonyl-edited ^{13}C−^{1}H HSQC experiments in which only resonances from selective sets of residues were observed.

Over 80 pairs of correlations were observed in the complementary 3D HN(CO)CA and 3D HNCA experiments. However, because of the small dispersion in the backbone chemical shifts of SC-65369, the α-carbon correlations often failed to yield unambiguous sequential assignments. The situation was complicated by a number of atoms which give rise to two resonances (see Figure 2). A large number of ambiguities were removed by the use of the CBCA(CO)NH and CBCANH experiments, where more than 100 pairs of $C^{\alpha}-C^{\beta}$ correlations were observed (ca. 10% of these were later determined to be doubled resonances), and the HBHA-(CBCACO)NH experiment, where $C^{\alpha}H(i-1)-C^{\beta}H(i-1)$ cross-peaks were observed for over 90 residues. Fragments of 3−8 residues were grouped together using these correlations, and their identities in the primary sequence were assigned on the basis of residue type as deduced from C^{α}, C^{β}, $C^{\alpha}H$, and $C^{\beta}H$ chemical shifts (Grzesiek & Bax, 1993a). Further verification of residue type was obtained at a later stage of the analysis by use of C(CO)NH and H(CCO)NH experiments (e.g., see Figure 3). The majority of sequential assignments were confirmed in (HB)CBCA(COCA)HA and HCA(CO)N spectra. All $C^{\beta}H-C^{\beta}$ correlations for aromatic and Asn/Asp residues, as well as $C^{\gamma}H-C^{\gamma}$ correlations for Gln/Glu residues, were verified in carbonyl-edited 2D ^{13}C−^{1}H HSQC experiments (data not shown). A summary of interresidue main-chain connectivities is shown in Figure 4. All main-chain resonances have been assigned except for those of Pro-30 and the amide proton and nitrogen of Leu-27.

Side-Chain Sequential Assignments. After most of the backbone assignments were completed, side-chain ^{1}H and ^{13}C resonances were identified in 3D H(CCO)NH, C(CO)-NH, HCCH-COSY, and HCCH-TOCSY spectra. For many aliphatic side chains, the assignments were made directly from the many carbon and hydrogen resonance frequencies

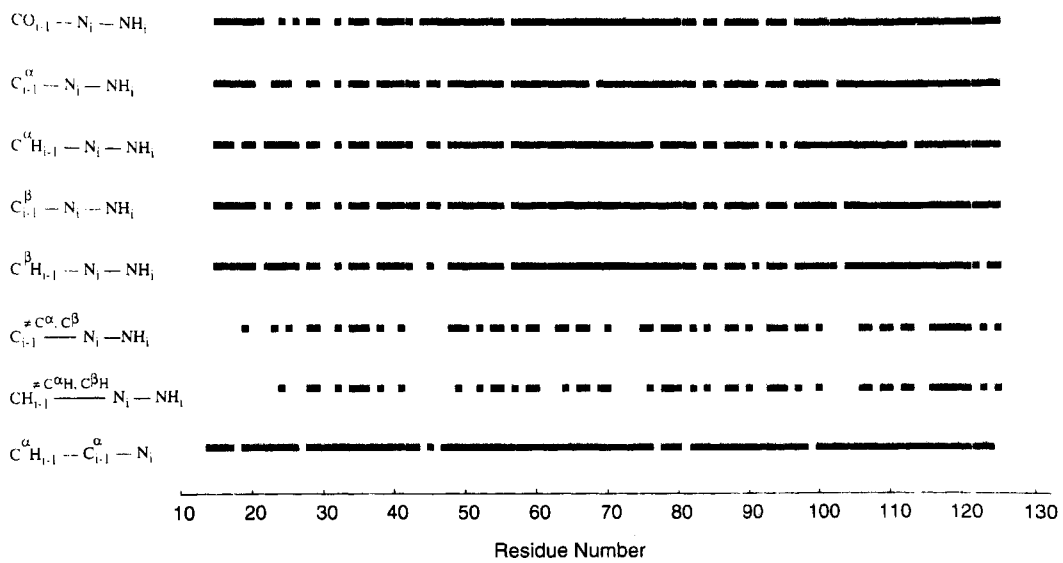

FIGURE 4: Summary of sequential scalar connectivities observed in the 3D triple-resonance experiments for SC-65369. The CO(i−1)−N(i)−NH(i) correlations were observed in the HNCO spectrum, $C^{\alpha}(i-1)-N(i)$-NH(i) and $C^{\beta}(i-1)-N(i)-NH(i)$ correlations in CBCA-(CO)NH and/or C(CO)NH spectra, $C^{\alpha}H(i-1)-N(i)-NH(i)$ and $C^{\beta}H(i-1)-N(i)$-NH(i) correlations in HBHA(CBCACO)NH and/or H(CCO)NH spectra, $C^{\neq\alpha/\beta}(i-1)-N(i)-NH(i)$ correlations in the C(CO)NH spectrum, $C^{\neq\alpha/\beta}H(i-1)-N(i)-NH(i)$ correlations in the H(CCO)-NH spectrum, and $C^{\alpha}H(i-1)-C^{\alpha}(i-1)-N(i)$ correlations in the HCA(CO)N spectrum.

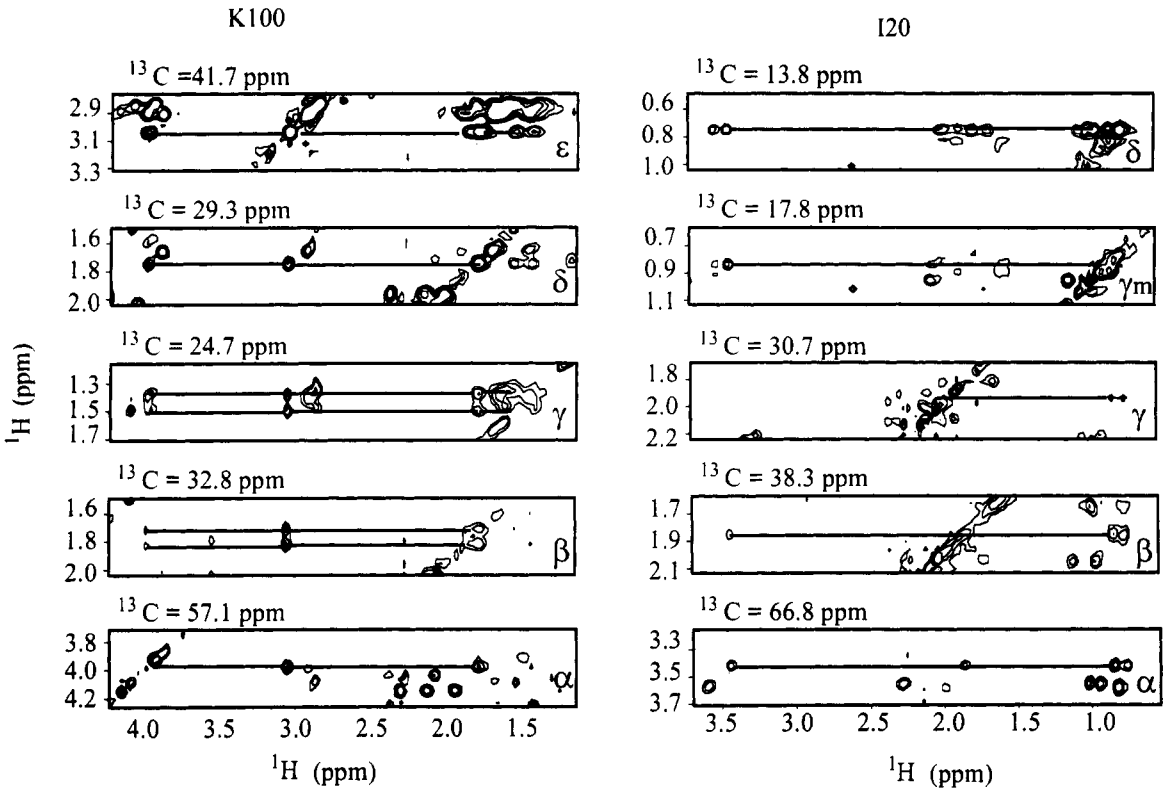

FIGURE 5: Slices of the 3D HCCH-TOCSY spectrum (mixing time 23 ms) illustrating the scalar connectivities observed for Lys-100 and Ile-20.

determined during the main-chain assignments. Examples of Lys-100 and Ile-20 spin systems are illustrated in Figure 5. One of the Met-45 $C^{\gamma}H_2$ resonances displays an unusual upfield shift, which was later determined by long-range NOEs to be due to its proximity to the Phe-113 side chain.

The splitting of some side-chain resonances made their assignments more difficult. Although most of the heterogeneity involved small differences in chemical shifts, some pairs of side-chain signals displayed large differences. For example, Leu-68 had two sets of side-chain resonances with large differences in both proton ($\Delta\delta_H \sim 0.4$ ppm) and carbon ($\Delta\delta_C \sim 1$ ppm) frequencies. The magnitude of these differences may be explained by the proximity of the leucyl isobutyl group to the indole of Trp-104, as revealed in the subsequent analysis of NOESY experiments; ring current effects could translate subtle differences in the relative orientation of the leucine alkyl and tryptophan aromatic ring into large chemical shift differences. Although the side-chain to main-chain correlations were largely missing for Leu-68, its side-chain resonances were assigned by the NOE between the δ-methyl and amide proton resonances.

Aromatic side-chain resonances were assigned by a combination of the traditional 2D ^{1}H-COSY and ^{1}H-TOCSY spectra and the 3D ^{13}C-edited NOESY spectrum. The side-chain amide resonances of three Gln residues were assigned on the basis of correlations observed in 3D C(CO)NH and H(CCO)NH experiments. Similar correlations for the 11 Asn side chains could not be unambiguously assigned due to severe spectral overlap. However, the side-chain amide resonances for seven Asn residues (at positions 15, 41, 52, 57, 70, 80, 105), as well as the ϵ-methyl groups of Met-19 and Met-49, were assigned on the basis of NOE correlations. The ^{1}H, ^{13}C, and ^{15}N resonance assignments are summarized in Table 2 in the Supplementary Material. Both main-chain and side-chain assignments are nearly complete.

Secondary Structure of SC-65369. Measured NMR parameters are time- and population-weighted averages, which can lead to difficulties in their interpretation (Jardetzky & Roberts, 1981). The use of a consensus of several NMR secondary structural indices, each with a different physical origin and averaging characteristics, helps to reduce the uncertainty in the assignment of secondary structure. Characteristic patterns of NOE connectivities constitute the most important means of identifying backbone structure in proteins (Wüthrich, 1986). Also widely used, $^3J_{NH\alpha}$ coupling constants relate to secondary structure by their dependence on the backbone dihedral angle ϕ via a Karplus-type relationship. Protection of amide protons against exchange with solvent deuterons has a drastically longer time scale than the first two methods. Patterns of protection against exchange infers hydrogen bonding in stable backbone structures, and these patterns can be diagnostic for elements of secondary structure. Finally, a method for calculating a consensus index of secondary chemical shifts has been developed by correlating secondary structure with the deviation of C^{α}, C^{β}, CO, and $C^{\alpha}H$ chemical shifts from their random-coil values (Spera & Bax, 1991; Wishart et al., 1992; Wishart & Sykes, 1994).

Using 3D ^{15}N- and ^{13}C-edited NOESY experiments, it was possible to assign the secondary structure of SC-65369 from the short- and medium-range NOEs. As outlined above, the assessment of the secondary structure was further assisted by $^3J_{NH\alpha}$ and backbone amide hydrogen exchange data as well as by a consensus index of secondary chemical shifts of C^{α}, C^{β}, CO, and $C^{\alpha}H$ resonances. A summary of the short- and medium-range NOEs is shown in Figure 6, along

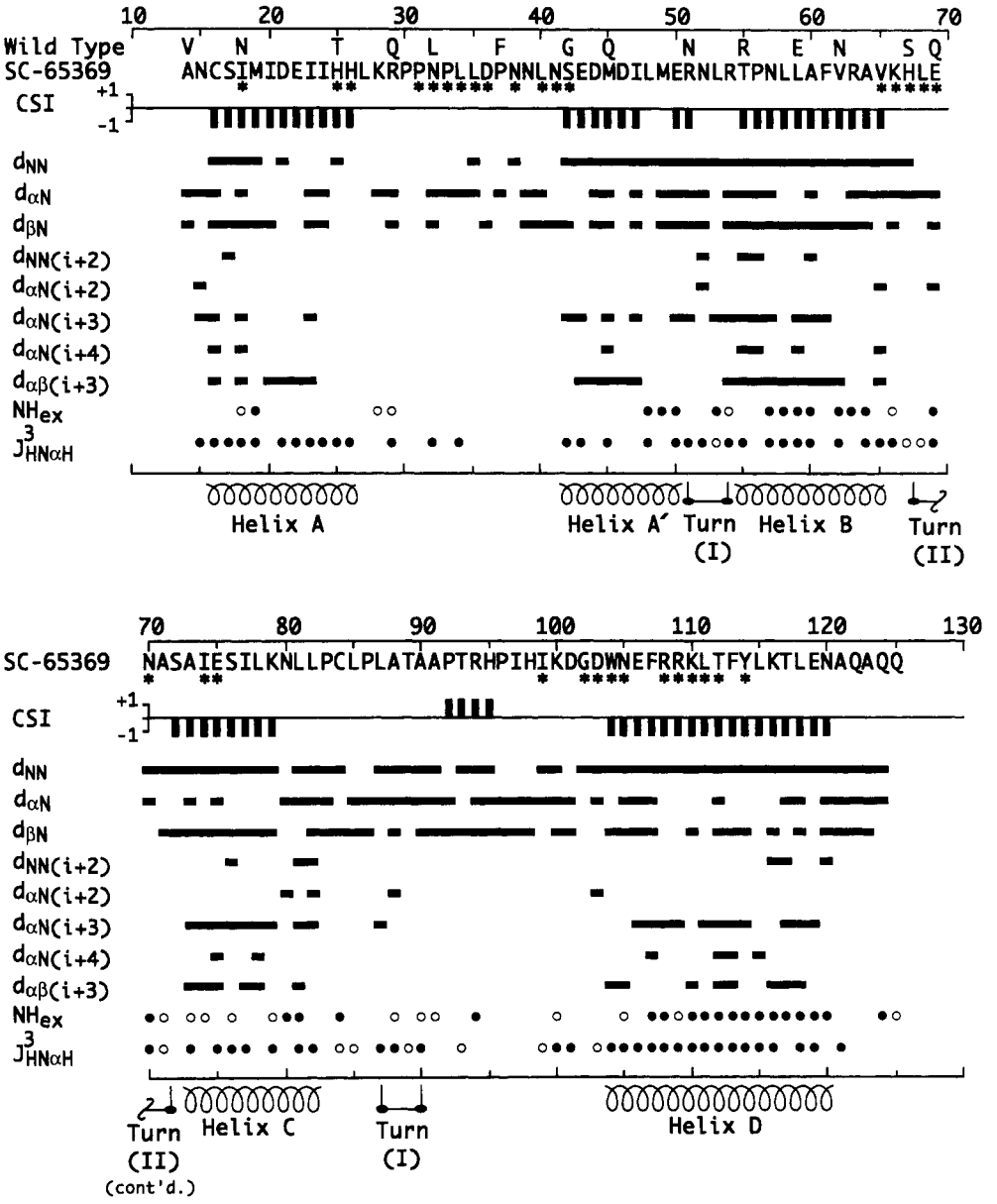

FIGURE 6: Summary of the sequential and medium-range NOEs observed for NH, $C^{\alpha}H$, and $C^{\beta}H$ in SC-65369. In the case of proline residues, the NOEs indicated for NH protons actually represent NOEs that were observed for the proline $C^{\delta}H$. Also indicated are the amide protons that were observed in the 2D $^{15}N-^{1}H$ HSQC spectra recorded after dissolving into D_2O buffer (○, detected after 10 min of exchange, but not at 29 h; ●, detected after 29 h of exchange), those $^{3}J_{HN\alpha}$ coupling constants that are smaller than 6 Hz (●) or larger than 8 Hz (○), the secondary chemical shift consensus index (CSI) calculated from the ^{13}C (C^{α}, C^{β}, CO) and ^{1}H ($C^{\alpha}H$) chemical shifts, and a summary of the secondary structural assignments made on the basis of the above information (see text). The sequence of SC-65369 is shown with an asterisk under those residues that exhibit heterogeneity. Mutation sites in SC-65369 are indicated by the wild-type residue placed directly above it. (Note that there are no substitutions in the C-terminal half of the sequence.)

with $^{3}J_{NH\alpha}$, the locations of slowly exchanging amide protons, and the consensus index of secondary chemical shifts. For all resolved resonances that exhibit heterogeneity, the NOE pattern for the two sets of signals is similar, thus indicating that there is no significant difference in the secondary structure of the species that originate these pairs of resonances.

Five helical segments can be deduced in this protein. Beginning at Cys-16, helix A is defined by sequential NH(i)−NH(i+1) and medium-range $C^{\alpha}H(i)$−NH(i+3) and $C^{\alpha}H(i)-C^{\beta}H(i+3)$ NOEs that are seen through His-26 (Figure 7A). Although many of the $^{3}J_{NH\alpha}$ in this fragment cannot be measured precisely, they are consistent with a helical conformation. Assignment of His-26 as the last residue of helix A relied on a combination of the secondary C^{α}, CO, and $C^{\alpha}H$ chemical shifts of Leu-27 and the absence of a characteristic helical $C^{\alpha}H(24)-C^{\beta}H(27)$ NOE connectivity. Because the Leu-27 amide proton and nitrogen resonances were unassigned, it was not possible to use either $^{3}J_{NH\alpha}$ or the existence of NH(26)−NH(27) and $C^{\alpha}H(24)$−NH(27) NOEs as a means to assess the conformational state of residue 27.

Residues 27−41 lack NOE connectivity patterns associated with regular secondary structure. A second stretch of helical structure (helix A′) is located between residues 42 and 50 on the basis of the NOE connectivities (Figure 7B). The large value of $^{3}J_{NH\alpha}$ for Leu-53 (9.4 Hz), combined with NOEs between NH(i)−NH(i+1) in Arg-51 through Arg-54, between $C^{\alpha}H(i)$−NH(i+3) of Arg-51 and Arg-54, and between NH(i)−NH(i+2) and $C^{\alpha}H(i)$−NH(i+2) of Asn-52

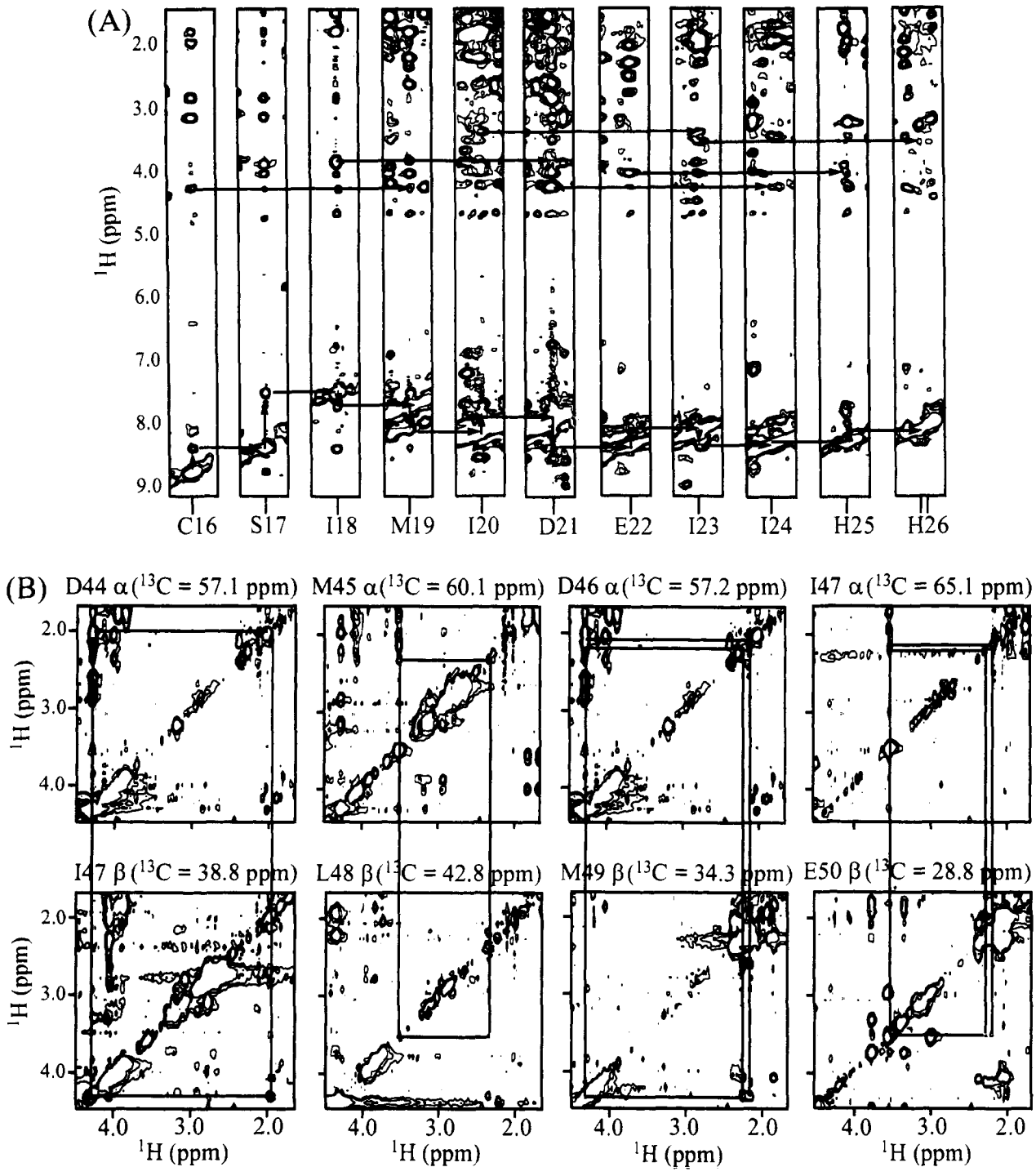

FIGURE 7: (A) Slices of the 3D ^{15}N-edited NOESY spectrum illustrating the sequential connectivities between Cys-16 and His-26. The NH(i)−NH(i+1), and C$^{\alpha}$H(i)−NH(i+3) cross-peaks are indicated with solid lines. The two NH signals observed for H26 are indicated by two vertical bars at the bottom of the H26 ^{15}N slice. (B) Slices of the 3D simultaneous ^{13}C,^{15}N-edited NOESY spectrum illustrating the C$^{\alpha}$H(i)−C$^{\beta}$H(i+3) connectivities between Asp-44 and Glu-50.

and Arg-54, defines residues 51−54 as a type I reverse turn. The slow amide hydrogen exchange rate of Arg-54 provides further support to the assignment of a reverse turn conformation to these residues.

Immediately following the reverse turn is a third helix that spans Thr-55 to Val-65 (helix B). Secondary chemical shifts are consistent with termination of this helix at Lys-66. For residues 68−71, a type II reverse turn is indicated by an NH(i)−NH(i+1) NOE between Asn-70 and Ala-71, a C$^{\alpha}$H-(i)−NH(i+2) NOE between Glu-69 and Ala-71, the small $^3J_{NH\alpha}$ of Glu-69 and Asn-70 (4.8 and 6.0 Hz, respectively), and the slow amide hydrogen exchange behavior of Ala-71.

The type II turn leads to a fourth helix in SC-65369 (helix C). Sequential and medium-range NOEs are readily observed in the segment between Ala-73 and Cys-84, while $^3J_{NH\alpha}$ larger than expected for a helical dihedral angle ϕ are observed for Ile-74 (6.7 Hz), Asn-80 (6.8 Hz), and Cys-84 (8.2 Hz). The consensus secondary chemical shift index suggests that the helix extends only to Lys-79. We tentatively refer to residues 73−82 as helix C, with possible distortions at Ile-74 and Asn-80. Following an irregular region spanning residues 83−86, another type I reverse turn

can be identified between Leu-87 and Ala-90. This turn is defined by NOEs between the NH(i)−NH(i+1) in Leu-87 through Ala-90, between the C$^{\alpha}$H(i)−NH(i+3) of Leu-87 and Ala-90, and by the large value of the amide proton−α proton coupling constant of Thr-89 (9.5 Hz) as well as by the hydrogen exchange data. A β-strand conformation is suggested by the chemical shift index method for residues 92−95; however, this assignment is not supported by the $^3J_{NH\alpha}$ coupling constants observed in this fragment (<5 Hz for Arg-94 and 7.6 Hz for His-95), nor is there any pattern of long-range NOEs indicative of a β-sheet.

The sequence beyond residue 95 lacks regular secondary structure until Trp-104, where a fifth helix begins (helix D). The consensus chemical shift index suggests that helix D ends at Asn-120, while the helical NOE pattern extends to Gln-122. The $^3J_{NH\alpha}$ coupling constant of Thr-117 (7.1 Hz) is larger than expected for a helical conformation, and beginning at Gln-122, the $^3J_{NH\alpha}$ coupling constants are about 7 Hz, which is also incompatible with a fixed helical conformation. Also noteworthy is that resonances for residues Ala-121 to Gln-125 become significantly narrower, indicating additional flexibility at the C-terminus. We thus refer to residues 104−120 as helix D, although deviation from a helical conformation may exist at Thr-117 and beyond.

The secondary structure of IL-3 has been studied using circular dichroism (CD) and sequence-based prediction methods (Freeman et al., 1991; Lokker et al., 1991; Kaushansky et al., 1992). Native hIL-3 was estimated to be about 40−50% helical from its far-UV CD spectra. The helicity of hIL-3 determined by CD is in good agreement with the NMR assignments reported here for SC-65369, viz., 50% helix (56 of 112 residues), which is reduced to 42% helix when the results for the truncated SC-65369 are extrapolated to the full length hIL-3 (i.e., 56 of 133 residues). In a recent report (Kaushansky et al., 1992), the secondary structure of hIL-3 was analyzed using the prediction algorithms of Garnier (1978), Parry et al. (1988), Chou and Fasman (1978), and Gascuel and Golmard (1988). Although each method predicted a helical protein, only the Parry method correctly predicted all four helices of the four-helical bundle (i.e., helices A, B, C, and D), but it failed to predict the existence of helix A′. On the other hand, the Garnier and Chou−Fasman methods correctly predicted which residues would be helical, including the sequence corresponding to helix A′, but it placed them in four helices instead of five, viz., residues 17−29, 41−51, 57−78, and 103−125. The key difference between the predictions and experimental results is the reverse turn at residues 68−71, which breaks the predicted helical stretch from residues 57 to 78 into helix B and C. This emphasizes the difficulty of relying on predictive methods since it would be impossible to correctly model the four-helix bundle motif from the Garnier and Chou−Fasman predictions made by Kaushansky et al. (1992). Residues 68−71 of SC-65369 have only one conservative substitution (Gln-69 → Glu-69), and thus this turn is likely to exist in the native protein. The molecule studied here is a truncated variant of hIL-3 with 14 mutations scattered more or less evenly throughout the N-terminal half of the protein. Significant structural change, especially large-scale change, is unlikely since the variant protein retains full bioactivity.

Proline Residues and Spectral Heterogeneity in SC-65369. It has been noted that the $^{13}C^{\alpha}$ chemical shifts of residues preceding prolines are often upfield-shifted relative to their random coil positions (Torchia et al., 1975; Clore et al., 1990). In SC-65369, the $^{13}C^{\alpha}$ chemical shifts of six of the nine residues preceding prolines (Arg-29, Asn-32, Asp-36, Leu-85, Ala-91, and His-95) exhibit upfield shifts, while two others (Thr-55 and Leu-82) exhibit downfield shifts; the later two residues are in helical segments. The ninth residue, Pro-30, cannot be assessed because its main-chain atoms were not assigned.

Many residues displaying chemical shift heterogeneity (see Figure 6; e.g., His-25, His-26, Pro-31, Asn-32, Pro-33, Leu-34, Leu-35, Asp-36, Asn-38 and Leu-40) are located in a region of sequence which contains four proline residues (positions 30, 31, 33 and 37).[2] Chemical shift heterogeneity caused by *cis*−*trans* isomerization of peptide bonds preceding proline residues has been described for staphylococcal nuclease (Evans et al., 1987; Hinck et al., 1990), calbindin D_{9k} (Chazin et al., 1989; Koerdel et al., 1990), salmon calcitonin (Amodeo et al., 1994), and anthopleurin-A (Scanlon & Norton, 1994). For calbindin D_{9k} and calcitonin, the heterogeneity was eliminated by substituting other amino acids for the prolines involved in isomerization; the effect of substitution for proline was not reported for anthopleurin-A. The activation energy barrier for isomerization of Xaa-Pro peptide bonds in peptides and proteins is in the range of 15−20 kcal/mol, and interconversion on the NMR time scale frequently requires elevated temperature. Chemical exchange spectroscopy was able to detect conformational exchange at 52 °C for staphylococcal nuclease (Alexandrescu et al., 1989), 80 °C for calbindin D_{9k}, 37 °C for calcitonin, and 42 °C for anthopleurin-A. Salmon calcitonin, anthopleurin-A, and calbindin D_{9k} had NOE connectivities characteristic of a mixture of *cis* and *trans* configurations, which further established that the two major conformational forms of these proteins differed by isomerization about Xaa-Pro peptide bonds. In the case of calcitonin, the *cis*−*trans* equilibrium depended on the polarity of the solvent, and the *cis* form was minimized in the presence of 0.9 M SDS. A similar chemical shift heterogeneity was observed in spectra used to determine the solution structure of G-CSF (Werner et al., 1994), and proline *cis-trans* isomerization was suggested as an explanation, although evidence of the kind discussed here was not reported.

Unfortunately, SC-65369 unfolds between 50 and 60 °C, and exchange spectroscopy performed at 50 °C failed to yield exchange cross-peaks, presumably because not enough thermal energy was available to traverse the activation energy barrier. NOE connectivities consistent with *trans* peptide bonds (Xaa NH to Pro C$^{\delta}$H) were seen for prolines 56, 83, 86, 92, and 96 of SC-65369; no *cis* peptide bond NOEs (Xaa C$^{\alpha}$H to Pro C$^{\alpha}$H) were identified. Diagnostic NOE connectivities for either *cis* or *trans* Xaa-Pro peptide bonds could not be found for prolines 30, 31, 33, and 37, either because of a lack of resonance assignments or because of severe spectral crowding, or both. As with the other proteins discussed above, site-directed mutagenesis offers another

[2] Although Pro-37 is a nonnative residue, this additional proline appears unlikely to be responsible for the heterogeneity because a related variant with a non-proline substitution at position 37 has similar spectral heterogeneity (Y. Feng, unpublished results).

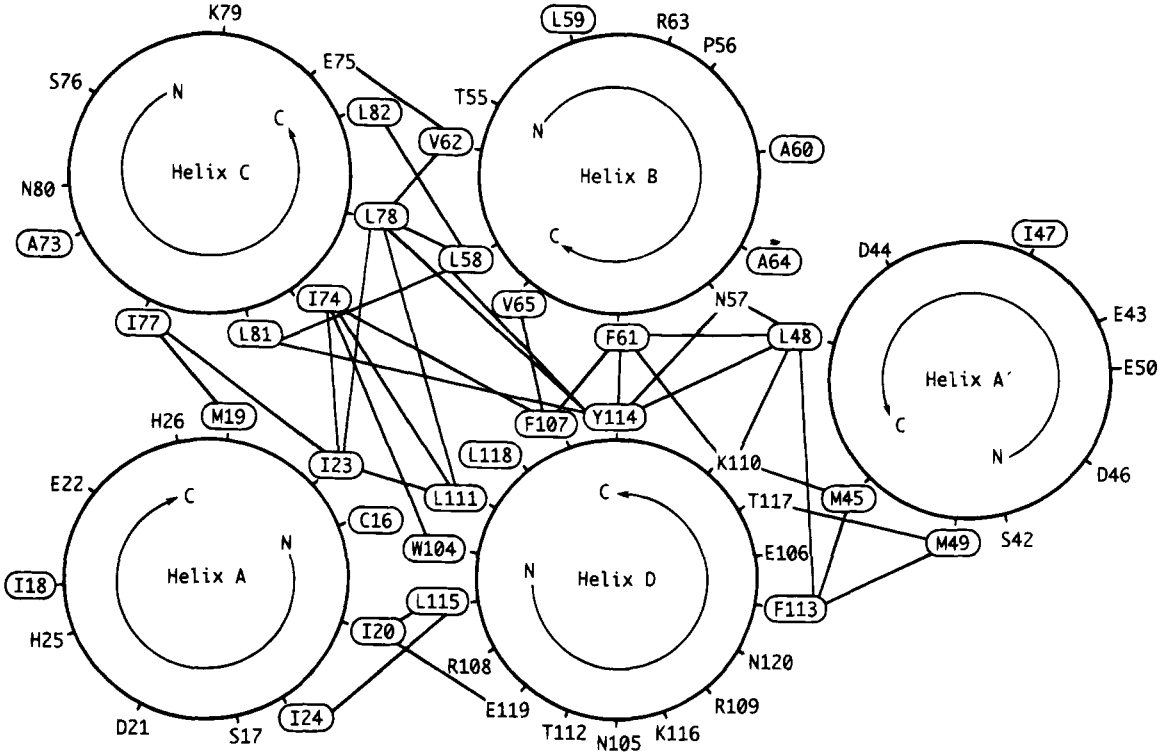

FIGURE 8: Schematic drawing of the packing of the five helices in SC-65369. Helix A and helix B are viewed from their N-termini, while helix A′, helix C, and helix D are viewed from their C-termini. The lines connect pairs of residues for which long-range NOEs have been observed for one or more pairs of their protons. Hydrophobic residues are enclosed in the ovals.

means to establish the significance of proline residues in the observed heterogeneity and the mutation of individual proline residues in hIL-3 variants is in progress. In addition to delineating the origin of the heterogeneity, these mutants will enable us to investigate whether the conformational felxibility of hIL-3 is important for its biological function.

Backbone Topology of SC-65369. Numerous long-range NOEs observed in ^{13}C- and ^{15}N-edited NOESY spectra indicate that the overall topology of SC-65369 adopts the distinct pattern observed in many cytokine structures, that is, an up-up-down-down, left-handed four-helical bundle. As in the case of the secondary structure, no distinct differences in the long-range NOE connectivities can be established for sites that exhibit heterogeneity, suggesting that although a significant number of residues display heterogeneous chemical shifts, the effect on conformation must be rather localized.

The largely amphipathic character of all five helices in SC-65369 is illustrated through the use of helical wheel projections (Figure 8). The single disulfide bond between Cys-16 and Cys-84 connects helix A and helix C. NOEs observed between one or more pairs of protons in Met-19 and Ile-77, Ile-23 and Ile-74, and Leu-27 and Ile-74 confirm that these two helices are antiparallel. For helix A and helix D, NOEs between pairs of protons in Ile-20 and Leu-115, Ile-20 and Glu-119, and Ile-23 and Leu-111 indicate that these helices are also antiparallel. For helix B, interproton NOEs observed between residues Leu-58 and Leu-81, Val-62 and Leu-78, Val-65 and Ala-71, as well as Asn-57 and Tyr-114, Val-62 and Leu-111, and Val-65 and Phe-107, establish that this helix is antiparallel to both helix C and helix D. Helix A′ displayed NOEs from Met-45 to Phe-113, and Met-49 to Phe-113 and Thr-117, thus indicating that helix A′ is parallel to helix D. This orientation is consistent with the relative orientation of the other helices

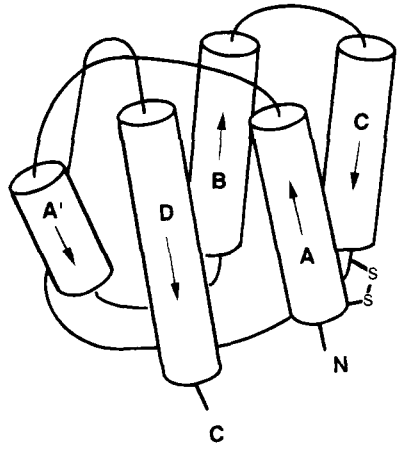

FIGURE 9: Schematic drawing of the three-dimensional structure of SC-65369.

discussed above. No long-range NOEs could be identified between helix A and helix B, between helix A and helix A′, or between helix A′ and helix C. The helical wheel projections shown in Figure 8 summarize these long-range NOEs. As expected from the amphipathic nature of these helices, their hydrophobic faces give rise to interhelical NOEs, which provide evidence of a hydrophobic core. On the basis of the long-range NOEs described in Figure 8, the global fold of SC-65369 is illustrated schematically in Figure 9 as a four-helical bundle structure in which there is the addition of helix A′ in the loop connecting helix A to helix B. The overall fold of SC-65369 is reasoned to be quite similar to native hIL-3 because the CD spectra indicate that they have comparable helical contents (Freeman et al., 1991; R. Schilling, unpublished results) and also because SC-65369 has proliferative and receptor binding activities similar to the wild-type protein (P. Olins, C. Bauer, and J. Thomas,

unpublished results). In comparing the fold of SC-65369 with the crystal structures of GM-CSF (Diederichs et al., 1992) and IL-5 (Milburn et al., 1993), the most striking difference is the additional helix (helix A′) which occurs just before helix B and is absent from the corresponding structures of both GM-CSF and IL-5.

IL-3, GM-CSF, and IL-5 bind to different low affinity cell surface receptors, called α-subunits, without eliciting the cellular response that leads to proliferation. High affinity binding and signal transduction is conferred by the formation of a complex between the cytokine−α-subunit complex and a common signal transducing subunit, the β-subunit. Significant binding to the β-subunit does not appear to occur in the absence of the low affinity α-subunit. Because these proteins bind to a common β-subunit, but to different α-subunits, the region corresponding to helix A′ may be important for cytokine-receptor recognition and specificity. A detailed analysis of the NMR data to determine the three-dimensional solution structure of SC-65369, and its functional aspects in light of extensive mutagenesis results, will be presented elsewhere.

ACKNOWLEDGMENT

We thank Chris Bauer for cloning and expression of pMON 13302 and for isotopic labeling of SC-65369, Mark Walker for assistance with protein purification, Kevin Duffin and Gary Lange for tryptic mapping and mass spectral analysis, Christine Smith for N-terminal sequencing, Ann Abegg for bioassay of NMR samples, and Roger Schilling for recording CD spectra of several hIL-3 variants. The assistance of the Monsanto St. Louis NMR Consortium was especially important for this work, and special thanks are due to Drs. Bill Hutton, John Kotyk, and John Likos. We thank Professor Lewis Kay of the University of Toronto for providing us with many pulse sequences and for helpful discussions on their implementation. Assistance with computer programming was provided by Norm Hoffman and John Roman. We thank Chris Bauer and Dr. Chuck Baum for critical comments on the manuscript. We also gratefully acknowledge the advice and encouragement of Dr. John McKearn and the Synthokine Project Team.

SUPPLEMENTARY MATERIAL AVAILABLE

Two tables listing data collection and processing parameters for each NMR experiment and the ^{1}H, ^{13}C, and ^{15}N resonance assignments of SC-65369 (9 pages). Ordering information is given on any current masthead page.

REFERENCES

Abdel-Meguid, S. S., Shieh, H.-S., Smith, W. W., Dayringer, H. E., Violand, B. N., & Bentle, L. A. (1987) *Proc. Natl. Acad. Sci. U.S.A. 84*, 6434−6437.

Amodeo, P., Morelli, M. A. C., & Motta, A. (1994) *Biochemistry 33*, 10754−10762.

Bax, A., Clore, G. M., Driscoll, P. C., Gronenborn, A. M., Ikura, M., & Kay, L. E. (1990) *J. Magn. Reson. 87*, 620−627.

Bazan, J. F. (1992) *Science 257*, 410−412.

Biesma, B., Willemse, P. H. B., Mulder, N. H., Sleijfer, D. Th., Gietema, J. A., Mull, R., Limburg, P. C., Bourma, J., Vallenge, E., & de Vries, E. G. E. (1992) *Blood 80*, 1141−1148.

Bodenhausen, G., & Ruben, D. J. (1980) *Chem. Phys. Lett. 69*, 185−189.

Chazin, W. J., Koerdel, J., Drakenberg, T., Thulin, E., Brodin, P., Grundstroem, T., & Forsen, S. (1989) *Proc. Natl. Acad. Sci. U.S.A. 86*, 2195−2198.

Chou, P. Y., & Fasman, G. D. (1978) *Adv. Enzymol. Relat. Areas Mol. Biol. 47*, 45−148.

Clore, G. M., Bax, A., Driscoll, P. C., Wingfield, P. T., & Gronenborn, A. M. (1990) *Biochemistry 29*, 8172−8184.

Denzlinger, C., Walther, J., Wilmanns, W., & Gerhartz, H. H. (1993) *Blood 81*, 2466−2468.

de Vos, A. M., Ultsch, M., & Kossiakoff, A. A. (1992) *Science 255*, 306−312.

Diederichs, K., Boone, T., & Karplus, P. A. (1991) *Science 254*, 1779−1782.

Evans, P. E., Dobson, C. M., Kautz, R. A., Hartfull, G., & Fox, R. O. (1987) *Nature 329*, 266−268.

Forman-Kay, J. D., Gronenborn, A. M., Kay, L. E., Wingfield, P. T., & Clore, G. M. (1990) *Biochemistry 29*, 1566−1572.

Freeman, J. J., Parr, G. R., Hecht, R. I., Morris, J. C., & McKearn, J. P. (1991) *Int. J. Biochem. 23*, 353−360.

Ganzer, A. (1993) *Cancer Invest. 11*, 212−218.

Ganzer, A., Lindemann, A., Seipelt, G., Ottman, O. G., Hermann, F., Eder, M., Frisch, J., Schulz, G., Mertlesmann, R., & Hoelzer, D. (1990) *Blood 76*, 666−676.

Garnier, J. (1978) *J. Mol. Biol. 120*, 97−120.

Gascuel, O., & Golmard, J. L. (1988) *Comput. Appl. Biosci. 4*, 357−365.

Goodall, G. J., Bagley, C. J., Vadas, M. A., & Lopez, A. F. (1993) *Growth Factors 8*, 87−97.

Grzesiek, S., & Bax, A. (1992a) *J. Am. Chem. Soc. 114*, 6291−6293.

Grzesiek, S., & Bax, A. (1992b) *J. Magn. Reson. 99*, 201−207.

Grzesiek, S., & Bax, A. (1993a) *J. Biomol. NMR 3*, 185−204.

Grzesiek, S., & Bax, A. (1993b) *J. Magn. Reson. 101*, 114−119.

Haak-Frendscho, M., Arai, N., Arai, K.-I., Baeza, M. L., Finn, M., & Kaplan, A. P. (1988) *J. Clin. Invest. 82*, 17−20.

Herrmann, F., Brugger, W., Kanz, L., & Mertelsmann, R. (1992) *Semin. Oncol. 19*, 422−431.

Hill, C. P., Osslund, T. D., & Eisenberg, D. (1993) *Proc. Natl. Acad. Sci. U.S.A. 90*, 5167−5171.

Hinck, A. P., Loh, S. N., Wang, J., & Markley, J. L. (1990) *J. Am. Chem. Soc. 112*, 9031−9034.

Ikura, M., & Bax, A. (1991) *J. Biomol. NMR 1*, 99−104.

Ikura, M., Kay, L. E., Tschudin, R., & Bax, A. (1990) *J. Magn. Reson. 86*, 204−209.

Jardetsky, O., & Roberts, G. C. K. (1981) *NMR in Molecular Biology*, Academic Press, Orlando, FL.

Kaushansky, K., Shoemaker, S. G., Broudy, V. C., Lin, N. L., Matous, J. V., Alderman, E. M., Aghajanian, J. D., Szklut, P. J., VanDyke, R. E., Pearce, M. K., & Abrams, J. S. (1992) *J. Clin. Invest. 90*, 1879−1888.

Kay, L. E. (1993) *J. Am. Chem. Soc. 115*, 2055−2057.

Kay, L. E., & Bax, A. (1990) *J. Magn. Reson. 86*, 110−126.

Kay, L. E., Ikura, M., Tschudin, R., & Bax, A. (1990) *J. Magn. Reson. 89*, 496−514.

Kitamura, T., Sato, N., Arai, K.-I., & Miyajima, A. (1991) *Cell 66*, 1165−1174.

Koerdel, J., Forsen, S., Drakenberg, T., & Chazin, W. J. (1990) *Biochemistry 29*, 4400−4409.

Lokker, N. A., Zenke, G., Strittmatter, U., Fagg, B., & Mora, N. R. (1991) *EMBO J. 10*, 2125−2131.

Lovejoy, B., Cascio, D., & Eisenberg, D. (1993) *J. Mol. Biol. 234*, 640−653.

Maniatis, T., Fritsch, E. F., & Sambrook, J. (1982) *Molecular Cloning. A Laboratory Manual*, p 68, Cold Spring Harbor Laboratory Press, Cold Spring Harbor, NY.

Marion, D., Driscoll, P. C., Kay, L. E., Wingfield, P. T., Bax, A., Gronenborn, A. M., & Clore, G. M. (1989a) *Biochemistry 28*, 6150−6156.

Marion, D., Kay, L. E., Sparks, S. W., Torchia, D. A. & Bax, A. (1989b) *J. Am. Chem. Soc. 111*, 1515−1517.

Marion, D., Ikura, M., Tschudin, R., & Bax, A. (1989c) *J. Magn. Reson. 85*, 393−399.

McKay, D. B. (1992) *Science 257*, 412−413.

Messerle, B. A., Wider, G., Otting, G., Weber, C., & Wüthrich, K. (1989) *J. Magn. Reson. 85*, 608−613.

Metcalf, D. (1991) *Science 254*, 529−533.

Milburn, M. V., Hassell, A. M., Lambert, M. H., Jordan, S. R., Proudfoot, A. E. I., Graber, P., & Wells, T. N. C. (1993) *Nature 363*, 172−176.
Miyajima, A., Mui, A. L.-F., Ogorochi, T., & Sakamaki, K. (1993) *Blood 82*, 1960−1974.
Mott, H. R., Driscoll, P. C., Boyd, J., Cooke, R. M., Weir, M. P., & Campbell, I. D. (1992) *Biochemistry 31*, 7741−7744.
Olins, P. O., Bauer, S. C., Braford-Goldberg, S., Sterbenz, K., Polazzi, J. O., Caparon, M. H., Klein, B. K., Easton, A. M., Paik, K., Klover, J. A., Thiele, B. R., & McKearn, J. P. (1995) *J. Biol. Chem.* (in press).
Pandit, J., Bohm, A., Jancarik, J., Halenbeck, R., Koths, K., & Kim, S.-H. (1992) *Science 258*, 1358−1362.
Parry, D., Minasian, E., & Leach, S. (1988) *Mol. Recognit. 1*, 107−110.
Pascal, S. M., Muhandiram, D. R., Yamazaki, T., Forman-Kay, J. D., & Kay, L. E. (1994) *J. Magn. Reson. B 103*, 197−201.
Powers, R., Gronenborn, A. M., Clore, G. M., & Bax, A. (1991) *J. Magn. Reson. 94*, 209−213.
Powers, R., Garrett, D. S., March, C. J., Frieden, E. A., Gronenborn, A. M., & Clore, G. M. (1992a) *Science 256*, 1673−1677.
Powers, R., Garrett, D. S., March, C. J., Frieden, E. A., Gronenborn, A. M., & Clore, G. M. (1992b) *Biochemistry 31*, 4334−4346.
Robinson, R. C., Grey, L. M., Staunton, D., Vankelecom, H., Vernallis, A. B., Moreau, J.-F., Stuart, D. I., Heath, J. K., & Jones, E. Y. (1994) *Cell 77*, 1101−1116.
Scanlon, M. J., & Norton, R. S. (1994) *Protein Sci. 3*, 1121−1124.
Schrader, J. W. (1986) *Annu. Rev. Immunol.*, 205−230.
Smith, L. J., Redfield, C., Boyd, J., Lawrence, G. M. P., Edwards, R. G., Smith, R. A. G., & Dobson, C. M. (1992) *J. Mol. Biol. 224*, 899−904.
Spera, S., & Bax, A. (1991) *J. Am. Chem. Soc. 113*, 5490−5492.
Tavernier, J., Devos, R., Cornelis, S., Tuypens, T., Van der Heyden, J., Fiers, W., & Plaetinck, G. (1991) *Cell 66*, 1175−1184.
Thomas, J. W., Baum, C. M., Hood, W. F., Klein, B. K., Monahan, J. B., Paik, K., Staten, N., Abrams, M., & McKearn, J. P. (1995) *Proc. Natl. Acad. Sci. U.S.A.* (in press).
Torchia, D. A., Leyerla, J. R., & Quattrone, A. J. (1975) *Biochemistry 14*, 887−900.
Walter, M. R., Cook, W. J., Ealick, S. E., Nagabhushan, T. L., Trotta, P. P., & Bugg, C. E. (1992) *J. Mol. Biol. 224*, 1075−1085.
Werner, J. M., Breeze, A. L., Kara, B., Rosenbrock, G., Boyd, J., Soffe, N., & Campbell, I. D. (1994) *Biochemistry 33*, 7184−7192.
Wishart, D. S., & Sykes, B. D. (1994) *J. Biomol. NMR 4*, 171−180.
Wishart, D. S., Sykes, B. D. & Richards, F. M. (1992) *Biochemistry 31*, 1647−1651.
Wlodawer, A., Pavlovsky, A., & Gutschina, A. (1992) *FEBS Lett. 309*, 59−64.
Wüthrich, K. (1986) *NMR of Proteins and Nucleic Acids*, Wiley, New York.
Yang, Y.-C., & Clark, S. C. (1990) *Int. J. Cell Cloning 8 (Suppl. 1)*, 121−129.
Yang, Y.-C., Ciarletta, A. B., Temple, P. A., Chung, P. S., Koviac, S. J., Witek-Giannotti, J. S., Leary, A. C., Kris, R., Donahue, R. E., Wong, G. G., & Clark, S. C. (1986) *Cell 47*, 3−10.
Zink, T., Ross, A., Ambrosius, D., Rudolph, R., & Holak, T. A. (1992) *FEBS Lett. 314*, 435−439.
Zink, T., Ross, A., Lüers, K., Cieslar, C., Rudolph, R., Holak, T. A. (1994) *Biochemistry 33*, 8453−8463.
Zuiderweg, E. R. P., & Fesik, S. W. (1989) *Biochemistry 28*, 2387−2391.

BI942824X